Total fusion cross section in ^{6}Li + ^{9}Be collisions

U. Umbelino,* R. Lichtenthäler Filho,† O. C. B. Santos, K. C. C. Pires, A. S. Serra, and A. Lépine-Szily
Instituto de Física, Universidade de São Paulo, São Paulo 05508-090, São Paulo, Brazil

(Received 8 December 2023; revised 12 March 2024; accepted 12 April 2024; published 7 May 2024)

Measurements of the ^{6}Li + ^{9}Be collision above the Coulomb barrier ($E_{\rm lab}$ = 11.2 MeV; $V_{\rm Cou}^{\rm lab}$ = 3.2 MeV) were performed using the ^{6}Li secondary beam selected by the RIBRAS (Radioactive Ion Beams in Brasil) first solenoid. The total reaction cross section was obtained from the ^{6}Li + ^{9}Be elastic scattering angular distribution, measured in the same experiment and analyzed by optical model calculations [U. Umbelino *et al.*, Phys. Rev. C **106**, 054602 (2022)]. Proton, deuteron, triton, and α yields were measured at angles around 45° in the laboratory and total fusion cross sections were deduced from the comparison between compound nucleus calculations and the measured light particle yields. The difference between the total reaction cross section and the obtained total fusion cross section provided an estimation of the contribution from other direct reaction mechanisms such as elastic and nonelastic breakup.

DOI: 10.1103/PhysRevC.109.054605

I. INTRODUCTION

The study of stable and exotic light nuclei at low energies has attracted much interest in recent years. Stable and exotic light nuclei such as ^{6,7,8}Li, ^{6}He, and ^{7,9}Be are weakly bound and present an α-cluster structure which makes them easily breakable in the collision with a target, affecting the balance between compound nucleus and direct reaction mechanisms in a way not yet totally understood [1–4]. Significant α-particle production has been observed in the collision of ^{6}Li on several targets [5–8], as well as in the ^{6}He + ^{120}Sn [9–11] and ^{6}He + ^{9}Be [12,13] systems, where α-particle production cross sections of the order of hundreds of millibarns have been reported [10,11]. On the other hand, large total reaction cross sections arise from the optical model analysis of the elastic scattering angular distribution for the same systems [10,12], when compared to systems with strongly bound projectiles, indicating that weakly bound and exotic light nuclei are more reactive than their strongly bound partners. The question whether the enhancement in the total reaction cross section is due to the direct reactions or compound nucleus cross sections, or both, remains open.

For light projectiles such as ^{6}Li, ^{6}He, and others it may not be trivial to separate compound nucleus and direct reactions by measuring only the charged particle production. In both cases, fragments such as α particles can be produced either in the projectile breakup or stripping reactions or from the compound nucleus evaporation, making it difficult to experimentally separate the two components. Reactions such as incomplete fusion can contribute to both compound and direct parts. In this case, a part of the projectile fuses with the target, forming an equilibrated system which will subsequently decay by the emission of protons, deuterons, tritons or α-particles, whereas the remaining projectile fragment continues all the way to the detector, presenting a typical energy and angular distribution of direct processes. Elastic scattering and breakup measurements for the ^{6}Li + ^{9}Be system have been reported previously [14], where a significant contribution of the compound nucleus formation was seen at backward angles.

Indeed, we expect that the angular and energy distributions of the particles will be quite different for direct and compound nucleus processes. The angular distributions for direct reactions are expected to peak at forward angles whereas, for the case of compound nucleus, they are more symmetric and contribute mainly at backward angles, where the direct processes cross sections are expected to be smaller. The projectile fragment energy distributions are also expected to be different. For the case of direct reactions such as the diffractive breakup, the fragments are emitted with velocities similar to the projectile and with energies around, or below, the projectile energy whereas particles from the compound nucleus decay are expected to have energy distributions shifted to lower energies.

Direct measurements of the compound nucleus formation and its sequential evaporation are performed using two different techniques. The first one consists of the detection of the characteristic γ radiation, emitted by the extremely excited compound system during its cooling process. This method has already been successfully used to obtain fusion cross sections of several systems, and, in some of those cases, the fusion cross section saturates the total reaction cross section [15–17], even at energies above the Coulomb barrier and involving weakly bound nuclei. The second method is the detection of the evaporated light particles, where the total fusion cross sections of light systems were obtained and are systematically smaller than the total reaction cross section [18,19]. Despite the difference in the energy range, comparison of the two techniques' measurements for the same system, such as ^{9}Be + ^{9}Be, indicates an enhancement of the direct processes'

*uiran@if.usp.br
†rubens@if.usp.br

intensities at higher energies [17,18]. In this work, we will present the measurements of light charged particles, such as protons, deuterons, tritons, and α's from the ^{6}Li + ^{9}Be collision at the $29^\circ \leqslant \theta_{\rm lab} \leqslant 61^\circ$ angular range. In this angular region, light particles such as protons and tritons are expected to come mainly from compound nucleus decay, whereas the deuterons and α's could have some contribution from direct processes involving the projectile or target breakup and transfer reactions.

This article has been organized as follows: in Sec. II we describe the experimental setup. In Sec. III we present proton, deuteron, and triton data analysis. In Sec. IV we show the cross section data and describe the compound nucleus calculations. In Sec. V we describe the calculation of evaporation and total fusion cross sections. In Sec. VI we present the α cross section, and in Sec. VII the conclusions are presented.

II. EXPERIMENTAL SETUP

The experiment was performed in the RIBRAS (Radioactive Ion Beams in Brasil) system [8,20–23] at the Nuclear Physics Open Laboratory of the Institute of Physics of the University of São Paulo. The 32 MeV ^{6}Li primary beam was provided by the Pelletron accelerator and impinged on the primary target, composed of a 3.6 cm cell sealed by two 2.04(2) μm Havar foils to maintain the ^{3}He gaseous target at 1014 mbar constant internal pressure. The primary target scattered the ^{6}Li particles to forward angles which were selected by the first RIBRAS solenoid and focused in the center of the central scattering chamber.

The reactions between the ^{6}Li beam and the primary target produced ^{3,4}He, ^{7}Be, and ^{8}B isotopes, which were also selected by the first solenoid. At the center of the central scattering chamber two secondary targets were mounted: a 1.92 mg/cm^2 ^{9}Be foil and a 4.5 mg/cm^2 gold target for normalization purposes. The first solenoid of the RIBRAS system has an amplification factor 1.5, implying that the secondary beam spot size will be 1.5× the primary beam spot size. The latter is of the order of 3–4 mm in our accelerator, so the secondary beam spot size would be of the order of 4–5 mm, well below the 2 cm diameter of the secondary target frame. Although we did not measured directly the effect of scattering in the secondary target frame in this experiment, we do not believe that this effect would affect by any means our results.

The detection system was composed by three ΔE-E silicon surface barrier telescopes. Telescope 2 was mounted to provide measurements of the elastic scattering at frontal angles; a thin ΔE (20 μm) was used in order to guarantee that the secondary beam did not stop in this detector and reach the E. Two telescopes (1 and 3), with a thicker ΔE (50 μm), were placed at 8.2 cm distance from the target at backward angles around $\theta_{\rm lab} = 45^\circ$ to detect the light particles emission. A set of rectangular collimators provided a 5 msr detection solid angle for telescope 2 and 9 msr for telescopes 1 and 3. The angular range, detector's thickness, collimator size, and detection solid angle are quoted in Table I.

A two-dimensional (ΔE–$E_{\rm Total}$) spectrum obtained by the secondary beam scattering in the gold target can be observed in Fig. 1, measured by telescope 2 at $\theta_{\rm lab} = 12^\circ$. Due to the fact that the collision in the gold target is pure Rutherford at this angle and energies, few reactions are expected and this spectrum shows basically the composition of the secondary beam. Telescope 2 (Fig. 1) shows the full identification and separation of all produced nuclei (^{3,4}He, ^{6}Li, ^{7}Be, and ^{8}B) without any ambiguity in the isotope identification. The full analysis of these elastic scattering experimental data (^{6}Li + ^{9}Be, ^{7}Be + ^{9}Be, and ^{8}B + ^{9}Be) was performed with optical model and coupled channels calculations [24].

TABLE I. Telescope information.

Tel.	Ang. range	ΔE (μm)	E (μm)	Col. size (mm)	$\Delta\Omega$ (msr)
1	42°–61°	50	1000	6 × 12	9
2	12°–31°	20	1000	3 × 12	5
3	29°–48°	50	1000	6 × 12	9

Figure 2 shows a typical spectrum obtained by telescope 1 at $\theta_{\rm lab} = 45^\circ$ with the gold (a) and beryllium (b) targets. The first one (a) shows some protons and ^{3}He at backward angles, where only light particles can surpass the thick ΔE detector. On the other hand, the second spectrum (b) shows a large yield of ^{1,2,3}H and α particles that cannot be observed in the ^{197}Au case, indicating that these nuclei have been produced in reactions with the ^{9}Be target. Furthermore, the spectrum (b) shows an empty region in the hydrogen isotopes yields at low energies. This effect is produced by the electronic threshold that ignores low amplitude signals in order to reduce the dead time of the acquisition system.

This experiment was performed with a cocktail beam of mainly ^{6}Li (see Table II), with contaminations of ^{3,4}He, ^{6}Li, ^{7}Be, and ^{8}B secondary beams. This fact imposes an evaluation of the particle yields that are produced by the reaction of each secondary beam contamination on the ^{9}Be target. For this reason, auxiliary measurements were performed without the ^{3}He gas in the primary target. The difference in the ^{6}Li energy in both cases, with and without gas in the target, is small, around 1%. Most of the energy loss in the primary target takes place in the 2 μm Havar windows so no correction in the solenoid current was made. The result, using the ^{197}Au

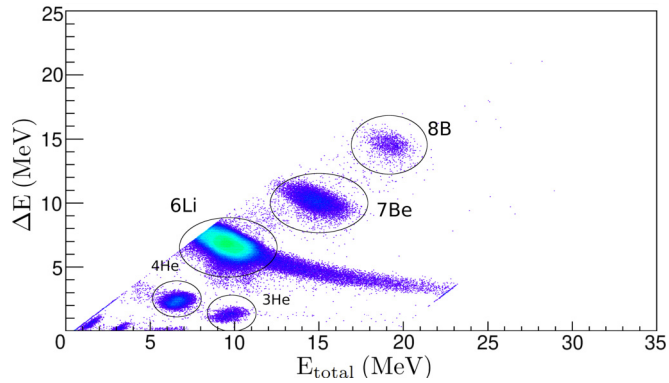

FIG. 1. Obtained ΔE-$E_{\rm Total}$ identification spectrum of the secondary beam scattered on a gold target at $\theta_{\rm lab} = 12^\circ$ for telescope 2.

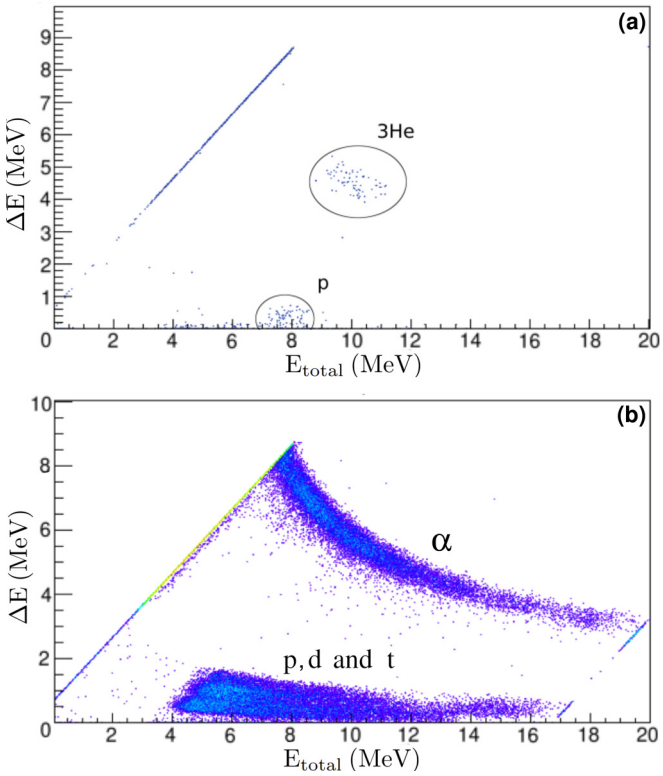

FIG. 2. Obtained ΔE–E_{Total} telescope 1 spectra of the secondary beam scattered on a gold (a) and a beryllium (b) target, both at $\theta_{\text{lab}} = 45^{\circ}$.

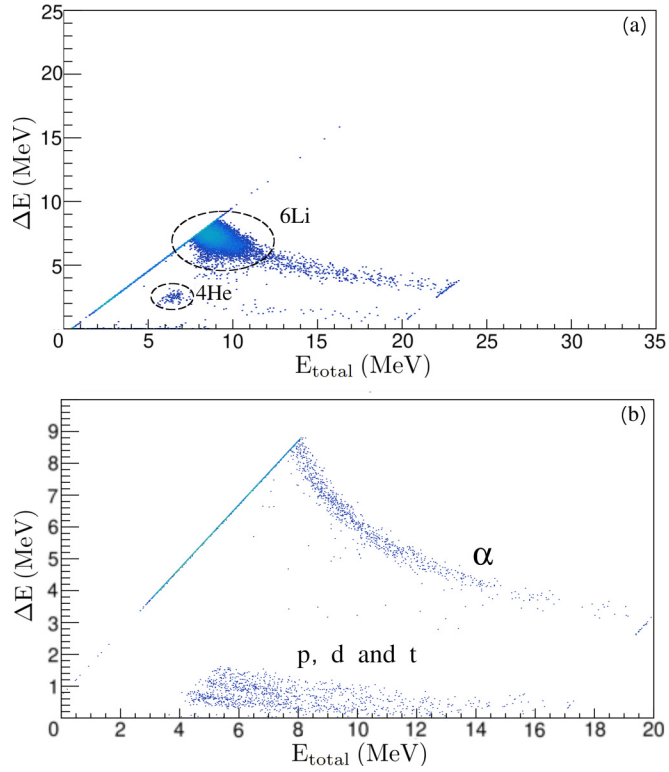

FIG. 3. Obtained ΔE–E_{Total} identification spectra of the secondary beam (without ^{3}He gas in the primary target) scattered on a gold target at $\theta_{\text{lab}} = 12^{\circ}$ for telescope 2 (a) and a beryllium target at $\theta_{\text{lab}} = 45^{\circ}$ for telescope 1 (b).

target and telescope 2 at $\theta_{\text{lab}} = 12^{\circ}$, can be seen in Fig. 3(a), where one can observe that the ^{3}He, ^{7}Be, and ^{8}B nuclei are not produced, but a strong presence of ^{6}Li and a much weaker ^{4}He can be noted. The Havar foils scatter the ^{6}Li; α particles and deuterons can be produced by the $^{6}\text{Li} \rightarrow {}^{4}\text{He} + d$ ($S_{\alpha} = 1.473$ MeV) breakup on the Havar foils. In Fig. 3(b) the result using the ^{9}Be target and the telescopre 1 at $\theta_{\text{lab}} = 45^{\circ}$ is presented. This spectrum is very similar to the the obtained with the cocktail beam in the same conditions [see Fig. 2(b)], but with less intensity. The main reason for this is that, without ^{3}He gas in the production target, the ^{6}Li current drops almost by a factor of 100.

The $^{6}\text{Li} + {}^{9}\text{Be}$ elastic scattering angular distribution was obtained and an optical model analysis was performed [24], providing a way to normalize the light particles produced in reactions with the ^{9}Be target. Through a comparison between this normalized light particles yields, with and without the ^{3}He target, it was concluded that almost 90% of the ^{1,2,3}H isotopes and around 60% of the α-particles yields come from the ^{6}Li beam (higher intensity). Only a small contribution from ^{4}He was reported, which is smaller than the experimental errors. These values were used to normalize the experimental cross sections. Therefore, the conclusion is that even using the cocktail beam, the ^{1,2,3}H particle production at backward angles is mainly due to the reaction between the ^{6}Li, higher intense secondary beam (see Table II), and the ^{9}Be target.

TABLE II. Average secondary beam intensities and energies (see text for more details).

Projectile	Intensity (pps)	E_{lab} (MeV)
^{3}He	7.2×10^{3}	10.1
^{4}He	4.1×10^{4}	7.6
^{6}Li	2.8×10^{6}	11.2
^{7}Be	3.6×10^{4}	17.3
^{8}B	4.0×10^{3}	23.7

III. DATA ANALYSIS

An important step in this analysis is to determine the secondary beam intensities in the scattering chamber. These quantities were obtained from the product $I = \epsilon \times i_p$, where ϵ is the production rate and i_p the ^{6}Li primary beam intensity, the latter measured by a Faraday cup located after the primary target and before the first solenoid. The value of ϵ for each projectile was calculated from measurements of the scattering of the secondary beam in the gold target, typically Rutherford at these energies and forward angles. The secondary beams intensities were periodically monitored at forward angles, making runs with a gold target interposed between the ^{9}Be runs. The energy of the secondary beam in the middle of the ^{9}Be target is obtained by the central value (E_{Total}) of the peak, corrected by the energy loss through the detection system and secondary target. The solenoid selection is determined by

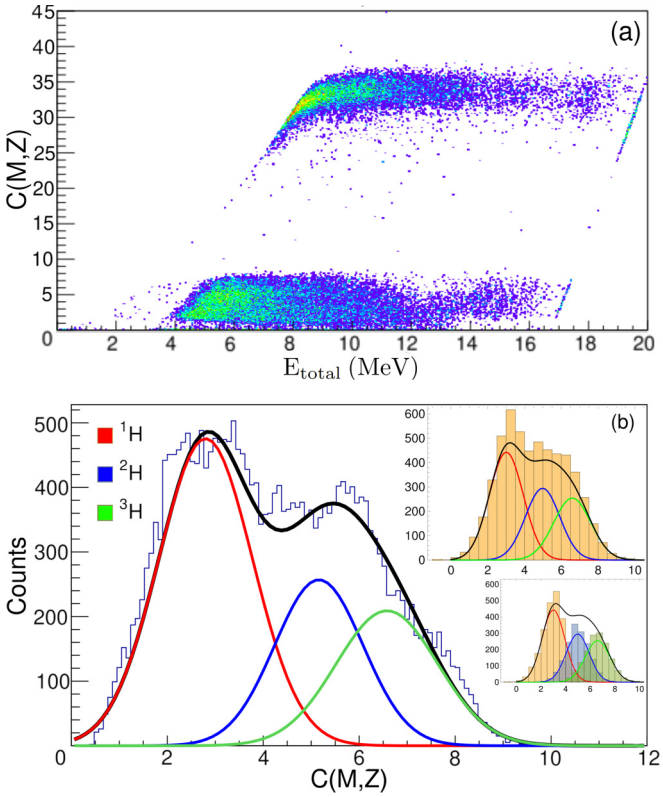

FIG. 4. $C(M,Z) \times E_{\text{Total}}$ spectra (a) and the $C(M,Z)$ projection (b), showing the comparison between the experimental (big) and simulated (medium and small) spectra, showing the separation of protons, deuterons, and tritons.

the magnetic rigidity and was used to validate the secondary beam energy. The secondary beam intensities and energies are presented in Table II.

We also analyzed the contamination of the experimental light particle yields due to the elastic scattering of the ^{1,2,3}H and ^{3,4}He contaminant beams observed in the experimental spectra on the gold target. For this purpose, we used the contaminant beam intensities, provided by the elastic scattering in the gold target, and theoretical cross sections, calculated by the double-folding São Paulo potential [25,26], to simulate the elastic scattering contributions. With this procedure, it was found that this contamination has an average value smaller than 3% for protons and 0.06% for ^{3}He, while the other particles do not reach the E detector and can not contaminate the biparametric spectra. Therefore, all elastic scattering contamination in the light particle yields would be smaller than the experimental uncertainties and has been neglected.

In Fig. 4 we present a two-dimensional spectrum of the light particles produced in reactions between the ^{6}Li secondary beam and the ^{9}Be target at $\theta_{\text{lab}} = 45^\circ$. The $C(M,Z) = (E_{\text{Total}})^b - (E_{\text{Total}} - \Delta E)^b$ value [27] was calculated and the $C(M,Z) \times E_{\text{Total}}$ spectra were built [Fig. 4(a)], where $b = 1.71$ was obtained through simulation. This method removes the typical hyperbolic behavior observed in the biparametric spectra ($\Delta E \times E_{\text{Total}}$) and presents the particle yields as straight horizontal lines. The projection of the

TABLE III. Proton, deuteron, and triton counts and multiplicities, obtained through Gaussian fit (m_{exp} and N_{Fit}) and calculations (m_{PACE} and N_{Simu}).

	m_{exp}	m_{PACE}	N_{exp}	N_{Simu}
^{1}H	0.470(5)	0.46	12975(130)	12707
^{2}H	0.254(5)	0.26	7011(144)	7182
^{3}H	0.206(4)	0.21	5702(95)	5801

p, d, and t yields on the $C(M,Z)$ axis is shown in Fig. 4(b). Furthermore, the production of protons, deuterons, and tritons was simulated with Monte Carlo method, employing the PACE [28] evaporation cross sections and multiplicities. The results are presented in the inset of Fig. 4(b), where the smaller one shows only a superposition of the particle yields and in the other the simulated spectra were summed. The light particle experimental distributions were fitted by Gaussian curves, whose parameters (mean value, variance, and area) were slightly varied around the values estimated by the simulation, to best fit the experimental data. The experimental (main image) and simulated (small images) data can be observed in Fig. 4(b). The emission rate of each particle can be used to provide an experimental estimation of the multiplicities. Table III presents the proton, deuteron, and triton yields and multiplicities, obtained experimentally (Gaussian fit) and by the simulation. As one can see, the results using the two methods are compatible with each other and reflect the same physical event.

Considering the deuteron yield, an important contribution could in principle come from the ^{6}Li breakup into a deuteron and α particle. A theoretical estimation of the ^{6}Li direct breakup cross section can be provided by continuum-discretized coupled-channel (CDCC) calculations. In Fig. 5, we compare the result of CDCC and PACE calculations, which indicate that only 5% of the deuteron production would come from ^{6}Li direct breakup, depending on the angular region. The full integrated differential cross sections provides about 297 mb for fusion and only 25 mb for breakup channels, so that the fusion channel seems to provide the major contribution to the deuteron yield and the contribution from the ^{6}Li breakup channel can be neglected within our error bars. Indeed, the direct breakup contribution is expected to be more important at forward angles, away from the angular region of the present measurements. On the other hand, it is worthwhile

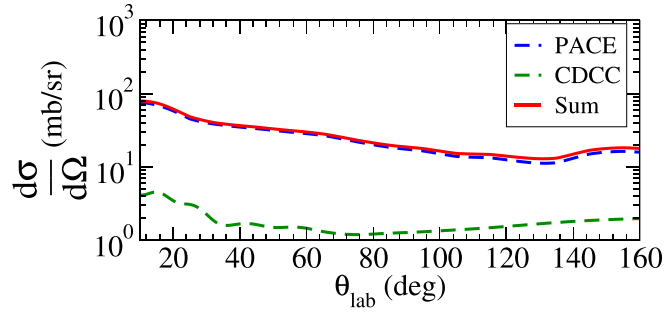

FIG. 5. CDCC predictions of the ^{6}Li breakup cross sections.

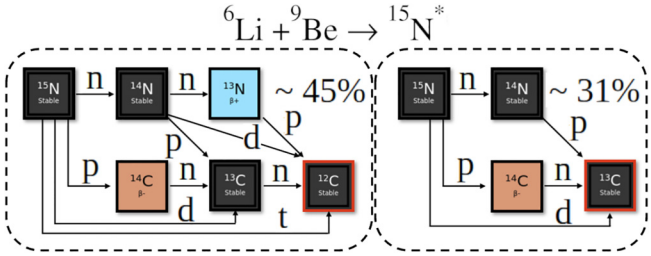

FIG. 6. Major evaporation chains of the ^{15}N* compound nucleus. The ^{12}C and ^{13}C isotopes represents almost 45% and 31% of the residual nuclei, respectively.

to mention that this is not the case for the the α-particle yield, which is strongly affected by inclusive breakup/transfer reactions as discussed in detail in Sec. VI. As we will show next, the light particles (protons, deuterons, and tritons) energy distributions do not seem to be significantly affected by the ^{6}Li breakup and are equally well reproduced by the same PACE calculations.

The PACE program performs a statistical calculation that takes into account the transmission coefficients, the nuclear level densities, and the complete fusion cross section. The transmission coefficients were calculated in the deexcitation steps through the optical model framework, where the nuclear potentials were obtained from standard literature, such as Perey-Perey [29] or Wilmore-Hodgson [30] compilations. The nuclear level densities were calculated with the Gilbert-Cameron formalism [31]. The complete fusion cross section acts as a normalization factor, that does not change the differential cross section shape but only proportionally enhances its value. Since there are no experimental measurements available, the fusion cross section was first configured as the total reaction cross section [$\sigma_R = 1107(16)$ mb], obtained by the optical model calculations [24]. The multiplicities are internally calculated by the ratio of the simulated particle emission yields and the number of produced compound nuclei. The agreement with the experimental data shows that the evaporation cascade, simulated by the PACE program, is realistic. Figure 6 shows the major evaporation chains calculated by the PACE, where almost of 76% of the ^{15}N* compound nucleus produces carbon isotopes (^{12,13}C) as residual nuclei. Table IV shows the most probable residual nuclei (RN) yields and the light particle (LP) multiplicities. As one can see, the theoretical result predicts that almost 76% of the ^{6}Li + ^{9}Be → ^{15}N* evaporation events produce

TABLE IV. Most probable residual nucleus (RN) yields and light particle (LP) multiplicities, estimated by PACE calculations.

	RN						
	^{14}N	^{14}C	^{13}C	^{12}C	^{8}Be	^{4}He	Others
Yield (%)	1.8	2.1	31	45	10	4.6	5.5
	LP						
	n	p	d	t	α	^{3}He	γ
m_{PACE}	0.88	0.46	0.26	0.21	0.24	>0.01	0.94

the ^{12}C or ^{13}C isotopes. Therefore, one can use the residual nuclei yields to infer information about the most probable evaporation chains of the ^{15}N* compound nuclei that emit the observed light particles.

The final step in the analysis is to obtain the energy distributions of the evaporated particles as the double differential cross sections, which were normalized by the scattering with the gold target:

$$\frac{d^2\sigma}{d\Omega\, dE}_{\text{Be}} = \frac{d\sigma}{d\Omega}^{\text{Ruth}}_{\text{Au}} \times \left[\frac{1}{\Delta E}\frac{N_c^{\text{Be}}}{N_c^{\text{Au}}}\frac{J^{\text{Be}}}{J^{\text{Au}}}\frac{N_t^{\text{Au}}}{N_t^{\text{Be}}}\frac{N_b^{\text{Au}}}{N_b^{\text{Be}}}\right], \quad (1)$$

where N_c is the count number in the peak of interest, J is the Jacobian from laboratory to center-of-mass framework, N_t is the areal density of the target, ΔE is the selected bin width (=1 MeV), and $\frac{N_b^{\text{Au}}}{N_b^{\text{Be}}}$ is taken equal to the ratio of the Faraday cup measurements in the corresponding runs, due to the fact that the production efficiencies are the same for both secondary targets. An interesting feature of this approach is the solid angle independence, which is canceled in the process. The experimental uncertainties were calculated taking into account the statistical errors of the Poisson distribution ($\sqrt{N}$) and a contribution due to the error in the target thickness (~5%).

IV. p, d, t ENERGY AND ANGULAR DISTRIBUTIONS

The experimental yield of the hydrogen isotopes was separated and the data were analyzed to obtain the double differential cross sections (energy distributions). In Fig. 7 we present the energy distributions of protons, deuterons, and tritons around $\theta_{\text{lab}} = 45^{\circ}$, compared with PACE calculations. The angular differential cross sections of the protons, deuterons, and tritons were obtained by the integration of the double differential cross sections in the full energy range. To perform the integration, the PACE results were normalized to represent the experimental data and were used as a theoretical model. The uncertainties were estimated by the different normalizations in the range between χ^2_{min} and $\chi^2_{\text{min}} + 1$. An additional source of uncertainty was taken into account, due to the large energy width of the ^{6}Li secondary beam (FWHM = 1.903 MeV). With this purpose, an additional contribution in the uncertainties was estimated as the standard deviation between all normalization values that were obtained by different PACE calculations in the energy range of the beam resolution. Figure 8 shows the experimental data of each hydrogen isotope evaporation. The theoretical results were normalized to best reproduce the experimental data, through the χ^2 minimization, and the fitted theoretical cross sections are presented as the red-line curves in both plots (Figs. 7 and 8). As one can see, both the experimental energy and angular distributions are well described by the PACE calculations in the energy region of the data, corroborating the method used to analyze the data. The normalization values [$N_p = 0.91(2)$, $N_d = 0.92(3)$, and $N_t = 0.88(2)$] are compatible with each other and an average value was obtained as 0.90(2). We kept error bars on the values obtained for the three particles.

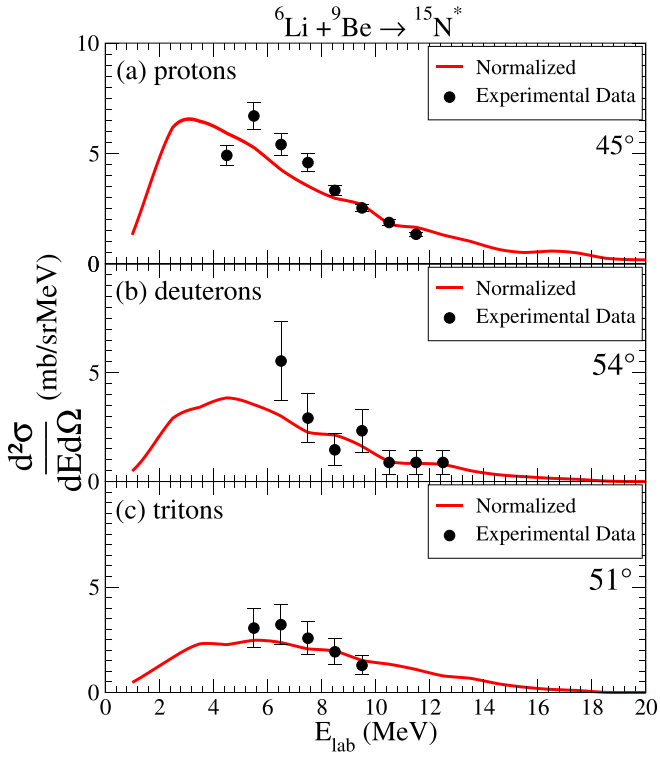

FIG. 7. Experimental energy distributions compared with the normalized [$N = 0.90(2)$] PACE calculations. See text for more details.

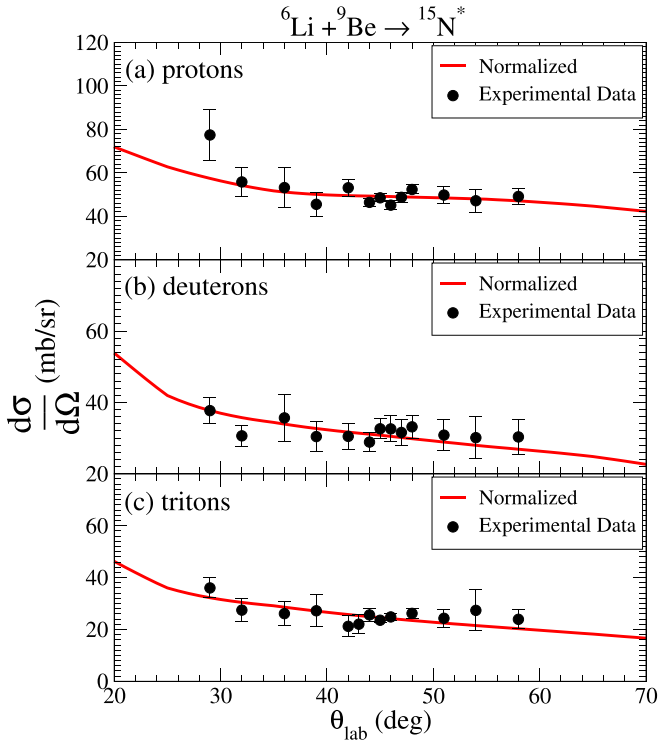

FIG. 8. Experimental angular distributions compared with the normalized [$N = 0.90(2)$] PACE calculations.

TABLE V. Evaporation and total fusion cross section of the compound system ^{6}Li + ^{9}Be.

^{6}Li + ^{9}Be → ^{15}N*	^{1}H	^{2}H	^{3}H	$\bar{\sigma}_f$	σ_{Wong}
σ_{evap} (mb)	461(10)	261(7)	202(5)		
σ_{TF} (mb)	1003(22)	1003(28)	961(25)	989(14)	1225
$\sigma_{\text{TR}}^{\text{MO}}$ (mb)				1107(16)	

V. EVAPORATION AND TOTAL (COMPLETE + INCOMPLETE) FUSION CROSS SECTIONS

Finally, experimental estimations of the evaporation cross sections of protons, deuterons, and tritons can be obtained through the integration of the normalized angular distributions. These quantities are related to the probability of each particle being evaporated by the formed compound nuclei. On the other hand, the particles multiplicities were statistically calculated by the ratio between emitted particle and compound nucleus formation numbers. Due to these facts, the evaporation cross sections and the particle multiplicities, that were validated by our analysis, can be used to estimate the total fusion cross section:

$$\sigma_{\text{TF}} = \frac{\sigma_{\text{evap}}}{m}. \tag{2}$$

The evaporation and total fusion cross sections were obtained and can be observed in Table V. It is notable that the estimated values, for all light particles, are consistent with each other and, due to this, a mean value was calculated. The total reaction cross section, obtained by optical model analysis (see Ref. [24]), is also shown and, as one can observe, is not much larger than the obtained total fusion cross section. An estimation of the total fusion cross section by Wong's formula [32] is included in Table V. These results indicate that total fusion plays a major role in the light particle production from the ^{6}Li + ^{9}Be reaction, well above the contribution from other direct processes such as breakup or transfer reactions. The difference between the total reaction and fusion cross sections from Table V gives 118(21) mb, which would be an estimation of the direct breakup plus transfer contributions to the light particle yields.

VI. α-PARTICLE DISTRIBUTION

In this section, we present an analysis of the helium strip, observed in the ΔE–E_{Total} spectra (Figs. 2 and 4). The projection of the α particle on the energy axis can be observed in Fig. 9 for $\theta_{\text{lab}} = 29^{\circ}$, together with PACE and IAV (Ichimura, Austern, and Vincent) calculations [33]. As one can observe, the predictions from the previous PACE calculations are significantly below the experimental α yield. It is expected, however, that since both ^{6}Li projectile and ^{9}Be target have a pronounced α structure, other direct reactions such as breakup or transfer could be contributing to the α yield, but are not explicitly taken into account in the PACE calculations. Among the possible candidates there is the ^{9}Be(^{6}Li, α)^{11}B* reaction. Due to well known Q optimum matching considerations, this kind of transfer reaction is favored to populate highly excited states of the recoil ^{11}B nucleus, providing scattered α particles

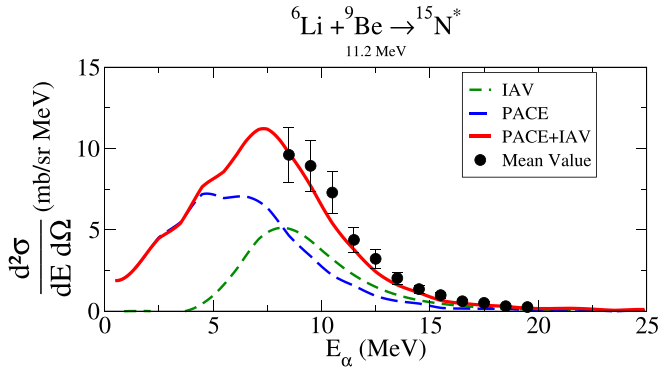

FIG. 9. Energy distribution of the α-particle yields at $\theta_{lab} = 29°$, compared with PACE and IAV calculations.

in an energy region that could match the measurements. The Ichimura, Austern, and Vincent (IAV) method is a parameter-free calculation which provides a highly accurate way to estimate the contribution of this kind of transfer/nonelastic-breakup reactions [33–37]. The main ingredients of the IAV model are the optical potentials in the entrance ^{6}Li + ^{9}Be and in the $d + {}^9$Be channels.

The ^{6}Li + ^{9}Be potential was obtained from reference [24] by reproducing the ^{6}Li + ^{9}Be elastic scattering angular distribution at the present bombarding energy. On the other hand, the $d + {}^9$Be potential must be in principle provided in the whole energy range involved in the transfer process, from zero up to the maximum deuteron energy of 3.73 MeV, given as 2/6 of the beam energy. However, in the present calculations we used a fixed $d + {}^9$Be potential obtained by extrapolating a deuteron global potential from Ref. [38]. The final $d + {}^9$Be Woods-Saxon (WS) parameters are given as $V = 71.5$ MeV, $r_0 = 1.17$ fm, $a_0 = 0.81$ fm, $W = 6.96$ MeV, $r_i = 1.56$ fm, and $a_i = 0.79$ fm; a WS imaginary surface $W_S = 6.21$ MeV, $r_S = 1.33$ fm, and $a_S = 0.56$ fm; and the Coulomb ($r_C = 1.69$ fm) potential. In addition, the binding $^6\text{Li} \to d + \alpha$ real potential was configured with a standard reduced nuclear radius and diffusivity ($r_0 = 1.25$ fm and $a_0 = 0.65$ fm), where the potential depth was varied to reproduce the $\alpha + d$ binding energy (1.473 MeV). The $\alpha + {}^9$Be potential was obtained from the Perey-Perey compilation [29]. Due to the lack of systematic optical potentials for the $\alpha + {}^{11}$B system, the $\alpha + {}^{10}$B parameters from [29] were used. For this calculation the interaction radii were calculated as performed in the original references: $R_i = r_i(A_p^{1/3} + A_t^{1/3})$ for the ^{6}Li + ^{9}Be and $d + \alpha$ interactions, and $R_i = r_i(A_t^{1/3})$ for the other potentials.

Finally, we performed the IAV calculation for the ^{9}Be(^{6}Li, α)^{11}B* reaction and the result is shown in Fig. 9. As one can see the PACE plus IAV theoretical results reproduce very well the observed experimental α yield at this angle. Furthermore, the total IAV cross section, integrated over energy and angle, provided almost 90 mb, which is statistically not very much different from the 118(21) mb difference between the total reaction and total fusion cross sections, estimated in the previous sections. At this point, we conclude that the α-particle yield is strongly contaminated by direct processes and cannot be used to estimate the fusion cross section.

VII. SUMMARY AND CONCLUSIONS

We performed measurements of ^{6}Li + ^{9}Be collisions using the ^{6}Li secondary beam produced by the RIBRAS facility. Energy distributions of light particles such as protons, deuterons, tritons, and α's were detected at backward angles $29° \leqslant \theta_{lab} \leqslant 61°$. Their experimental energy and angular distributions were compared with compound nucleus PACE calculations, supposing the complete fusion ^{6}Li + ^{9}Be → ^{15}N* process and decay. Proton, deuteron, triton, ^{3}He, and α particles were considered in the evaporation process of the compound nucleus. A very good agreement was obtained between the shape of the experimental energy and angular distributions of the three lighter particles (protons, deuteron, and tritons) and the PACE calculation, indicating that they were produced in the evaporation of an equilibrated compound system. The total fusion cross section of 989(14) mb for the ^{6}Li + ^{9}Be reaction was extracted from the comparison between the experimental proton, deuteron, and triton yields and the PACE calculations, taking into account the multiplicities of the decay particles.

A total ^{6}Li + ^{9}Be reaction cross section of 1107(16) mb was obtained from the elastic scattering angular distribution, which is only 118(21) mb above the total fusion cross section, indicating thatr this mechanism accounts for almost 90% the total reaction cross section. The sum of the predictions of the elastic and nonelastic breakup contributions, provided by CDCC and IAV calculations ($\sigma_{BU} + \sigma_{NBU} = 25 + 90 = 115$ mb), is in remarkable agreement with the remaining cross section [118(21) mb]. In contrast to the light particle measurements presented here, the α-particle yields were found to be considerably larger than the PACE predictions, indicating that direct processes, such as breakup or transfer, could be contributing in an important way to the α yields. IAV (Ichimura, Austern, and Vincent) calculations were performed for the ^{9}Be(^{6}Li, α)^{11}B* transfer reaction and the results show that this reaction could account for most of the observed α-yield excess.

Finally, we conclude that it seems to be possible to obtain reliable total fusion cross sections by measuring light particles such as protons, deuterons, and tritons evaporated at backward angles around $\theta_{lab} \approx 45°$. Although some contribution from direct processes in the deuteron line would be expected for the ^{6}Li + ^{9}Be system, due to the $\alpha + d$ projectile's structure, it was not observed in the present experiment, at least in the angular range of the present measurements. The α-particle yield, on the other hand, appears to be strongly contaminated by direct processes such as breakup and deuteron transfer reactions and cannot be used to estimate the fusion cross section.

ACKNOWLEDGMENTS

This work was supported by Coordenação de Aperfeiçoamento de Pessoal de Nível Superior–Brasil (CAPES); a part of the work was developed under the project INCT-FNA

Proc. No. 464898/2014-5, Fundação de Amparo à Pesquisa do Estado de São Paulo, FAPESP (Brazil), Contracts No. 2019/02759-0, No. 2019/07767-1, No. 2016/17612-7, No. 2013/22100-7, No. 2021/12254-3, and No. 2019/05769-7.

[1] N. Keeley, R. Raabe, N. Alamanos, and J. Sida, Fusion and direct reactions of halo nuclei at energies around the Coulomb barrier, Prog. Part. Nucl. Phys. **59**, 579 (2007).

[2] L. F. Canto, P. R. S. Gomes, R. Donangelo, J. Lubian, and M. S. Hussein, Recent developments in fusion and direct reactions with weakly bound nuclei, Phys. Rep. **596**, 1 (2015).

[3] J. J. Kolata, V. Guimarães, and E. F. Aguilera, Elastic scattering, fusion, and breakup of light exotic nuclei, Eur. Phys. J. A **52**, 123 (2016).

[4] A. Pakou, O. Sgouros, V. Soukeras, J. Casal, and K. Rusek, Reaction mechanisms of the weakly bound nuclei ^{6,7}Li and ^{7,9}Be on light targets at near barrier energies, Eur. Phys. J. A **58**, 8 (2022).

[5] A. Pakou, E. Stiliaris, D. Pierroutsakou, N. Alamanos, A. Boiano, C. Boiano *et al.*, Fusion cross sections of ^{8}B + ^{28}Si at near-barrier energies, Phys. Rev. C **87**, 014619 (2013).

[6] K. Pfeiffer, E. Speth, and K. Bethge, Break-up of ^{6}Li and ^{7}Li on tin and nickel nuclei, Nucl. Phys. A **206**, 545 (1973).

[7] F. A. Souza, C. Beck, N. Carlin, N. Keeley, R. Liguori Neto, M. M. de Moura *et al.*, Reaction mechanisms in the ^{6}Li + ^{59}Co system, Nucl. Phys. A **821**, 36 (2009).

[8] R. Lichtenthäler, O. C. B. Santos, A. Serra, U. Umbelino, K. C. C. Pires, J. R. B. Oliveira *et al.*, Experiments with $A = 6$–8 exotic beams in RIBRAS, Eur. Phys. J. A **57**, 92 (2021).

[9] P. N. de Faria, R. Lichtenthäler, K. C. C. Pires, A. M. Moro, A. Lépine-Szily, V. Guimarães *et al.*, Elastic scattering and total reaction cross section of ^{6}He + ^{120}Sn, Phys. Rev. C **81**, 044605 (2010).

[10] P. N. de Faria, R. Lichtenthäler, K. C. C. Pires, A. M. Moro, A. Lépine-Szily, V. Guimarães *et al.*, α-particle production in ^{6}He + ^{120}Sn collisions, Phys. Rev. C **82**, 034602 (2010).

[11] S. Appannababu, R. Lichtenthäler, M. A. G. Alvarez, M. Rodríguez-Gallardo, A. Lépine-Szily, K. C. C. Pires *et al.*, Two-neutron transfer in the ^{6}He + ^{120}Sn reaction, Phys. Rev. C **99**, 014601 (2019).

[12] K. C. C. Pires, R. Lichtenthäler, A. Lépine-Szily, V. Guimarães, P. N. de Faria, A. Barioni *et al.*, Experimental study of ^{6}He + ^{9}Be elastic scattering at low energies, Phys. Rev. C **83**, 064603 (2011).

[13] K. C. C. Pires, R. Lichtenthäler, A. Lépine-Szily, and V. Morcelle, Total reaction cross section for the ^{6}He + ^{9}Be system, Phys. Rev. C **90**, 027605 (2014).

[14] E. Muskat, J. Carter, R. W. Fearick, and V. Hnizdo, Inelastic scattering in the ^{6}Li + ^{9}Be system leading to unbound excited states of either nucleus, Nucl. Phys. A **581**, 42 (1995).

[15] C. J. S. Scholz, C. J. S. Scholz, and E. Kuhlmann, Complete fusion of ^{7}Li + ^{16}O in the region of the Coulomb threshold, Z. Phys. A **325**, 203 (1986).

[16] A. Mukherjee, U. Datta Pramanik, M. Saha Sarkar, A. Goswami, P. Basu, S. Bhattacharya *et al.*, ^{7}Li + ^{12}C and ^{7}Li + ^{13}C fusion reactions at subbarrier energies, Nucl. Phys. A **596**, 299 (1996).

[17] A. Mukherjee and B. Dasmahapatra, Fusion cross sections for ^{7}Li + ^{11}B and ^{9}Be + ^{9}Be reactions at low energies, Nucl. Phys. A **614**, 238 (1997).

[18] A. R. Omar, J. S. Eck, T. R. Ophel, and J. R. Leigh, Total fusion of ^{9}Be + ^{9}Be at $E(^{9}\text{Be}) = 35$–55 MeV, Phys. Rev. C **30**, 1516 (1984).

[19] J. F. Mateja, J. Garman, D. E. Fields, R. L. Kozub, A. D. Frawley, and L. C. Dennis, Fusion cross sections for four heavy-ion entrance channels leading to the ^{23}Na compound nucleus, Phys. Rev. C **30**, 134 (1984).

[20] R. Lichtenthäler, A. Lépine-Szily, V. Guimarães, C. Perego, V. Placco, O. Camargo, Jr. *et al.*, Radioactive Ion beams in Brazil (RIBRAS), Eur. Phys. J. A **25**, 733 (2005).

[21] A. Lépine-Szily, R. Lichtenthäler, and V. Guimarães, The Radioactive Ion Beams in Brazil (RIBRAS) facility, Eur. Phys. J. A **50**, 128 (2014).

[22] R. Lichtenthäler, M. A. G. Alvarez, A. Lépine-Szily, S. Appannababu, K. C. C. Pires, U. U. da Silva *et al.*, RIBRAS: The facility for exotic nuclei in Brazil, Few-Body Syst. **57**, 157 (2016).

[23] E. Leistenschneider, A. Lépine-Szily, M. A. G. Alvarez, D. R. Mendes, R. Lichtenthäler, V. A. P. Aguiar *et al.*, Spectroscopy of high-lying resonances in ^{9}Be by the measurement of (p, p), (p, d), and (p, α) reactions with a radioactive ^{8}Li beam, Phys. Rev. C **98**, 064601 (2018).

[24] U. Umbelino, R. Lichtenthäler, O. C. B. Santos, K. C. C. Pires, A. S. Serra, V. Scarduelli *et al.*, Quasielastic scattering of light radioactive and stable projectiles on ^{9}Be, Phys. Rev. C **106**, 054602 (2022).

[25] L. C. Chamon, B. V. Carlson, L. R. Gasques, D. Pereira, C. De Conti, M. A. G. Alvarez *et al.*, Toward a global description of the nucleus-nucleus interaction, Phys. Rev. C **66**, 014610 (2002).

[26] M. A. G. Alvarez, L. C. Chamon, M. S. Hussein, D. Pereira, L. R. Gasques, E. S. Rossi *et al.*, A parameter-free optical potential for the heavy-ion elastic scattering process, Nucl. Phys. A **723**, 93 (2003).

[27] G. F. Knoll, *Radiation Detection and Measurements* (Wiley, New York, 1989).

[28] A. Gavron, Statistical model calculations in heavy ion reactions, Phys. Rev. C **21**, 230 (1980).

[29] C. M. Perey and F. G. Perey, Compilation of phenomenological optical-model parameters 1954–1975, At. Data Nucl. Data Tables **17**, 1 (1976).

[30] D. Wilmore and P. Hodgson, The calculation of neutron cross-sections from optical potentials, Nucl. Phys. **55**, 673 (1964).

[31] A. Gilbert and A. G. W. Cameron, A composite nuclear-level density formula with shell corrections, Can. J. Phys. **43**, 1446 (1965).

[32] C. Y. Wong, Interaction barrier in charged-particle nuclear reactions, Phys. Rev. Lett. **31**, 766 (1973).

[33] M. Ichimura, N. Austern, and C. M. Vincent, Equivalence of post and prior sum rules for inclusive breakup reactions, Phys. Rev. C **32**, 431 (1985).

[34] O. C. B. Santos, R. Lichtenthäler, K. C. C. Pires, U. Umbelino, E. O. N. Zevallos, A. L. de Lara *et al.*, Evidence of the effect of strong stripping channels on the dynamics of the ^{8}Li + ^{58}Ni reaction, Phys. Rev. C **103**, 064601 (2021).

[35] O. C. B. Santos, R. Lichtenthäler, A. M. Moro, K. C. C. Pires, U. Umbelino, A. S. Serra *et al.*, One-neutron stripping from ^{8}Li projectiles to ^{9}Be target nuclei, Eur. Phys. J. A **59**, 14 (2023).

[36] J. Lei and A. M. Moro, Reexamining closed-form formulae for inclusive breakup: Application to deuteron- and ^{6}Li-induced reactions, Phys. Rev. C **92**, 044616 (2015).

[37] J. Lei and A. M. Moro, Comprehensive analysis of large α yields observed in ^{6}Li-induced reactions, Phys. Rev. C **95**, 044605 (2017).

[38] Y. Han, Y. Shi, and Q. Shen, Deuteron global optical model potential for energies up to 200 MeV, Phys. Rev. C **74**, 044615 (2006).